Metabolic Engineering Communications 7 (2018) e00076

Contents lists available at ScienceDirect

Metabolic Engineering Communications

journal homepage: www.elsevier.com/locate/mec

Harnessing a P450 fatty acid decarboxylase from *Macrococcus caseolyticus* for microbial biosynthesis of odd chain terminal alkenes

Jong-Won Lee[a,b,1], Narayan P. Niraula[c,1,2], Cong T. Trinh[a,b,c,*]

[a] Bredesen Center for Interdisciplinary Research and Graduate Education, University of Tennessee, Knoxville, TN, USA
[b] Center for Bioenergy Innovation, Oak Ridge National Laboratory, Oak Ridge, TN, USA
[c] Department of Chemical and Biomolecular Engineering, University of Tennessee, Knoxville, TN, USA

ARTICLE INFO

Keywords:
P450 decarboxylase
Terminal alkene
Protein homology modeling
Alanine scan
Escherichia coli
Macrococcus caseolyticus

ABSTRACT

Alkenes are industrially important platform chemicals with broad applications. In this study, we report a direct microbial biosynthesis of terminal alkenes from fermentable sugars by harnessing a P450 fatty acid (FA) decarboxylase from *Macrococcus caseolyticus* ($OleT_{MC}$). We first characterized $OleT_{MC}$ and demonstrated its in vitro H_2O_2-independent activities towards linear C10:0-C18:0 FAs, with higher activity for C16:0-C18:0 FAs. Next, we engineered a *de novo* alkene biosynthesis pathway, consisting of $OleT_{MC}$ and an engineered *E. coli* thioesterase (TesA) with compatible substrate specificities, and introduced this pathway into *E. coli* for terminal alkene biosynthesis from glucose. The recombinant *E. coli* EcNN101 produced a total of 17.78 ± 0.63 mg/L odd-chain terminal alkenes, comprising of 0.9% ± 0.5% C11 alkene, 12.7% ± 2.2% C13 alkene, 82.7% ± 1.7% C15 alkene, and 3.7% ± 0.8% C17 alkene, and a yield of 0.87 ± 0.03 (mg/g) on glucose. To improve alkene production, we identified and overcame the electron transfer limitation in $OleT_{MC}$, by introducing a two-component redox system, consisting of a putidaredoxin reductase (CamA) and a putidaredoxin (CamB) from *Pseudomonas putida,* into EcNN101, and demonstrated the alkene production increased ~2.8 fold. Finally, to better understand the substrate specificities of $OleT_{MC}$ observed, we employed *in silico* protein modeling to illuminate the functional role of FA binding pocket.

1. Introduction

Alkenes (or olefins) are industrially important platform chemicals used to manufacture polymers, lubricants, surfactants, and coatings (Lappin and Sauer, 1989). Alkenes are currently produced by the well-established chemical conversion route (e.g., hydrogen cracking) using petroleum-based feedstocks that are neither renewable nor sustainable (Ren et al., 2006; Mol, 2004). In recent years, there is great interest in developing microbial conversion routes to produce alkenes from renewable and sustainable sources, such as biomass-derived fermentable sugars (Rude et al., 2011; Beller et al., 2010; Mendez-Perez et al., 2011; Rui et al., 2014, 2015; Chen et al., 2015; Zhu et al., 2017).

Various species are known to produce alkenes endogenously via decarbonylation of aldehydes (Winters et al., 1969; Tornabene, 1982; Ladygina et al., 2006), decarboxylation of FAs (Görgen et al., 1990), condensation of unsaturated polyenes (Ney and Boland, 1987), and oxidation of FAs (Rui et al., 2015, 2014). Various types of alkenes can be synthesized including alkadienes (Liu et al., 2014; Mendez-Perez et al., 2014), terminal alkenes (or 1-alkenes) (Rude et al., 2011; Mendez-Perez et al., 2011; Rui et al., 2014) as well as non-terminal alkenes (Beller et al., 2010), depending on enzyme types and substrates employed. To date, a number of different classes of enzymes have been reported to synthesize terminal alkenes including a P450 FA decarboxylase/peroxygenase (OleT, belonging to the CYP152 family) (Rude et al., 2011), a type-I polyketide synthase-like enzyme (CurM/Ols) (Mendez-Perez et al., 2011), a desaturase-like enzyme (UndB) (Rui et al., 2015), and a non-heme oxidase (UndA) (Rui et al., 2014). These enzymes take various substrates (e.g., FAs, fatty aldehydes, or FA thioesters) to produce terminal alkenes with different carbon chain lengths. For instance, OleT, CurM/Ols, and UndB are capable of synthesizing (C6-C12) medium-chain and (> C12) long-chain alkenes while UndA only produces medium chain length alkenes. The diversity of these enzyme specificities can potentially offer unique opportunities to develop microbial cell factories to engineer designer olefins for tailored applications.

Among the putative P450 FA decarboxylases/peroxygenases dis-

* Corresponding author at: Department of Chemical and Biomolecular Engineering, University of Tennessee, Knoxville, TN, USA.
E-mail address: ctrinh@utk.edu (C.T. Trinh).
[1] Equal contributions.
[2] Current address: Pfizer Inc., Kalamazoo, MI, USA.

https://doi.org/10.1016/j.mec.2018.e00076
Received 16 June 2018; Received in revised form 23 July 2018; Accepted 23 July 2018

covered, $OleT_{JE}$ is the most well-characterized enzyme for alkene biosynthesis (Rude et al., 2011; Liu et al., 2014; Dennig et al., 2015; Belcher et al., 2014). $OleT_{JE}$ has broad substrate specificity for C12:0-C20:0 FAs in vitro, with the highest towards C12:0 FA in the presence of redox partner proteins and C14:0 FA in the H_2O_2 –dependent system (Liu et al., 2014). Currently, the underlying mechanism to control the substrate specificity of P450 FA decarboxylases (e.g., $OleT_{JE}$) is not fully understood for olefin biosynthesis with desirable specific chain lengths. Furthermore, for the low-cost, large-scale production of terminal alkenes, the use of H_2O_2-independent decarboxylases (e.g., $OleT_{JE}$) is likely favorable by avoiding the external supply and cytotoxicity of H_2O_2. Thus, exploring the enzyme diversity of H_2O_2–independent decarboxylases with different substrate specificities is important for understanding enzyme characteristics and developing protein/metabolic engineering strategies to enhance microbial production of terminal alkenes from biomass-derived sugars.

In this study, we identified and harnessed a novel P450 fatty acid (FA) decarboxylase from *M. caseolyticus* ($OleT_{MC}$) for terminal alkene biosynthesis. In particular, we first discovered in vitro H_2O_2-independent decarboxylase activities of $OleT_{MC}$ towards linear C10:0-C18:0 FAs, with higher activity for C16:0-C18:0 FAs. Next we established the *de novo* alkene biosynthesis pathway and demonstrated direct microbial production of terminal alkenes from glucose in an engineered *E. coli* strain (Fig. 1). We identified and overcame the electron transfer limitation in $OleT_{MC}$, by introducing a two-component redox system. By employing *in silico* protein modeling, we postulated a mechanism responsible for the observed substrate specificities of $OleT_{MC}$ that is distinct from the well-characterized $OleT_{JE}$.

2. Results and discussion

2.1. Genome mining of OleT decarboxylases for terminal alkene biosynthesis

To identify the putative H_2O_2-independent P450 FA decarboxylases, we performed genome mining, a combination of the sequence alignment and phylogenetic analysis, using the protein sequence of $OleT_{JE}$ (ADW41779) as a template. The sequences of the CYP152 P450 enzyme family (Rude et al., 2011) were first aligned to select the candidates that have the conserved catalytic site residues Phe79, His85, and Arg245 like $OleT_{JE}$ (Matthews et al., 2017). Among the 29 decarboxylase candidates, we found that three P450 enzymes from *M. caseolyticus* (WP_041635889.1), *Corynebacterium efficiens* (WP_011075937.1), and *Kocuria rhizophila* (WP_012399225.1) have the conserved catalytic site residues (Supplementary Fig. S1). Based on the phylogenetic analysis, we found that the P450 enzyme of *M. caseolyticus* (WP_041635889.1) is the closest ortholog to $OleT_{JE}$ with the highest amino acid identity (~60%) (Fig. 2 and Supplementary Fig. S1). Thus, we chose the P450 from *M. caseolyticus,* named $OleT_{MC}$, for further characterization.

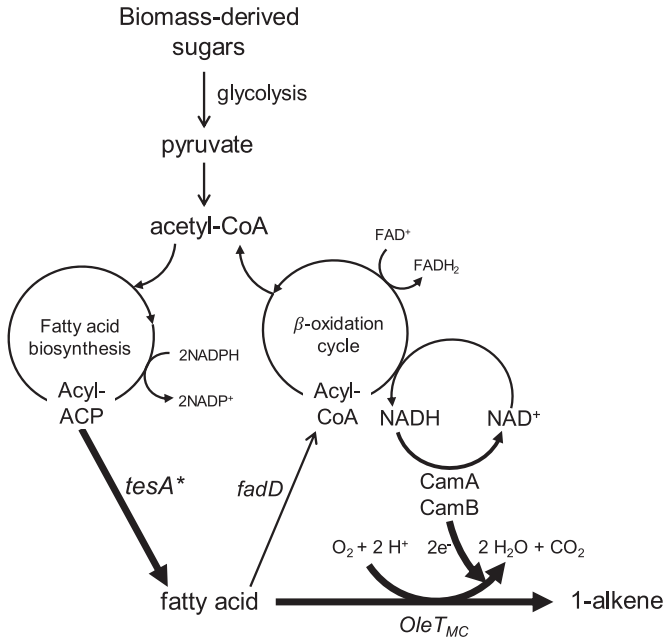

Fig. 1. Synthetic pathway for endogenous production of terminal alkenes in *E. coli*.

2.2. In vitro characterization of $OleT_{MC}$

The expression of $OleT_{MC}$ in BL21 (λDE3) pNN33 was confirmed in vivo with reddish cell cultures due to the heme-containing $OleT_{MC}$ and in vitro by a sodium dodecyl sulfate polyacrylamide gel electrophoresis (SDS-PAGE) and spectrophotometric analysis (Supplementary Fig. S2). After protein isolation, we performed the in vitro enzyme assay to examine the H_2O_2-independent decarboxylase activity of $OleT_{MC}$ towards linear, saturated FAs. The result shows that $OleT_{MC}$ could convert C10:0-C18:0 FAs to the corresponding odd chain terminal alkenes without H_2O_2 as an oxidant, confirmed by GC/MS (Supplementary Fig. S3). Under the H_2O_2-independent (O_2-dependent) conditions, $OleT_{MC}$ showed the highest specific activity towards C18:0 FA (1.13 ± 0.09 μM/min/mg) and the lowest specific activity towards C10:0 FA (0.17 ± 0.04 μM/min/mg) (Fig. 4A, Supplementary Table S1). $OleT_{MC}$ exhibited almost the same specific activity for C12:0 FA (0.62 ± 0.10 μM/min/mg) and C14:0 FA (0.66 ± 0.04 μM/min/mg). We did not observe the activity of $OleT_{MC}$ for < C10:0 FAs. The FA specificity of $OleT_{MC}$ can be ranked as follows: C18:0 > C16:0 > C14:0 ≥ C12:0 > C10:0. Taken altogether, $OleT_{MC}$ is a potential FA decarboxylase for developing the terminal alkene biosynthesis pathway in recombinant hosts (e.g., *E. coli*) for direct conversion of fermentable sugars to terminal alkenes.

2.3. Establishing the terminal alkene biosynthesis pathway in E. coli

We designed the heterologous terminal alkene biosynthesis pathway in *E. coli* BL21 (λDE3), consisting of two genes – the leaderless *tesA** gene encoding a thioesterase to convert acyl ACPs to FAs and the $OleT_{MC}$ gene encoding a decarboxylase to convert these FAs to terminal alkenes. We chose TesA* because it has higher specificities towards C16:0-C18:0 acyl ACPs than C12:0-C14:0 acyl ACPs (Bonner and Bloch, 1972) to produce corresponding FAs that are preferable substrates for $OleT_{MC}$. Fig. 3A-C shows kinetics of cell growth, sugar consumption, and product formation in shake flask experiments of the recombinant *E. coli* EcNN101 engineered to carry the terminal alkene biosynthesis pathway.

During the first 24 h of growth phase, EcNN101 could grow and produce odd terminal alkenes. At 24 h, cells completely consumed 20 g/L of glucose and entered the stationary phase with a biomass titer of 4.16 ± 0.07 g/L (Fig. 3A). Terminal alkene production peaked at a titer of 21.92 ± 0.69 mg/L, comprised of 4.5% ± 0.2% C11 alkene, 38.9% ± 1.1% C13 alkene, 55.4 ± 0.8% C15 alkene, and 1.2 ± 0.5% C17 alkene (Fig. 3B). Besides alkenes, the corresponding FAs were also produced at a much higher titer of 558.03 ± 18.95 mg/L, consisting of 24.9 ± 0.1% C12:0 FA, 41.0 ± 0.2% C14:0 FA, 25.2 ± 0.4% C16:0 FA, 7.6 ± 0.3% C18:0 FA, and 1.4 ± 0.1% C20:0 FA (Fig. 3C). The composition of these FAs correlated well with the specificity of TesA* (Bonner and Bloch, 1972). The relatively high FA production clearly implied that $OleT_{MC}$ was the rate-limiting step of the engineered terminal alkene biosynthesis pathway. The result also shows that the C15 alkene was produced at the highest level even though the fraction of C16:0 FA was lower than that of C14:0 FA and relatively similar to that of C12:0 FA. This result is consistent with the substrate preference of $OleT_{MC}$ towards C16:0 FA characterized in vitro and also implies

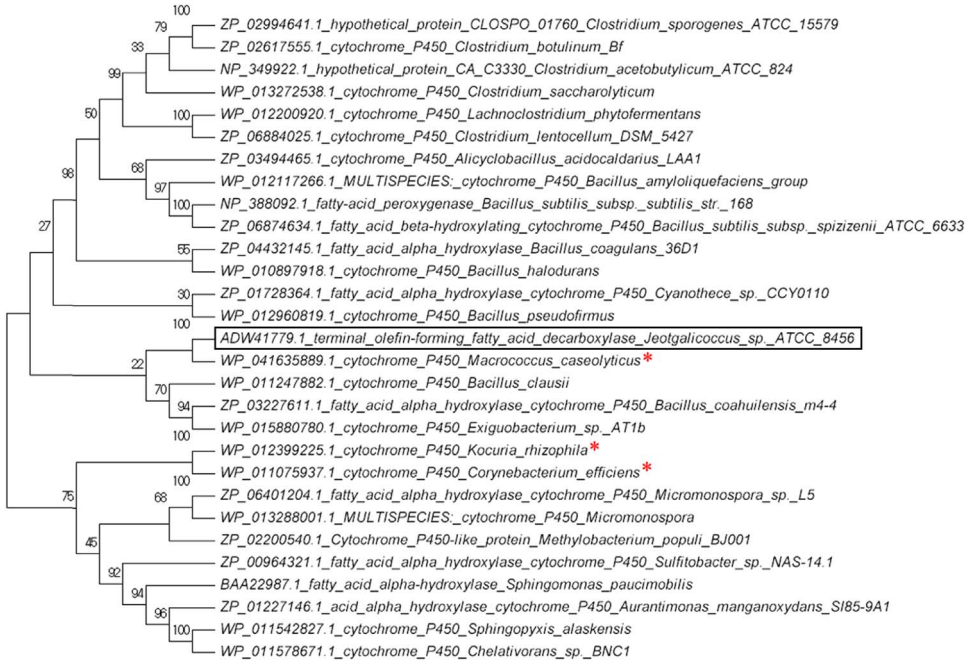

Fig. 2. Phylogenetic analysis of $OleT_{JE}$ with the CYP152 P450 enzyme family. $OleT_{JE}$ is shown in the box. The enzymes that have the conserved $OleT_{JE}$ catalytic site residues Phe79, His85, and Arg245 are marked with "* ".

that C16:0 FA was not limiting for decarboxylation. The production of C17 terminal alkene, however, was relatively low likely due to the low availability of C18:0 FA.

During the stationary phase (after 24 h), no glucose was available and about 398.15 ± 4.79 mg/L saturated FAs were consumed primarily for cell maintenance while cell concentration remained relatively constant. At 48 h, the alkene titer was slightly decreased to 17.78 ± 0.63 mg/L probably due to cell lysis and/or evaporation. The final alkene yield was 0.87 ± 0.03 mg/g. It is interesting to note that EcNN101 did not produce terminal alkenes during stationary phase even though degradation of saturated FAs, highly reduced substrates, could generate available NAD(P)H for FA decarboxylation via the β-oxidation pathway. This result implies that olefin production might be limited by the efficiency of electrons transferred to $OleT_{MC}$ for decarboxylation.

2.4. Improving terminal alkene production by enhancing electron shuttling to $OleT_{MC}$

It is known that the electron flow from NAD(P)H to the terminal P450 enzyme is facilitated by a two-component redox system such as ferredoxin reductase (FDR) and NAD(P)H-dependent ferredoxin (FDX). Most of the bacterial P450s belonging to the class I P450s use this two-component redox system for shuttling electrons (Peterson et al., 1990; Gunsalus and Sligar, 1978). We hypothesized that the $OleT_{MC}$ activity in EcNN101 might have been limiting during the stationary phase due to the lack of a two-component redox system. To test this hypothesis, we constructed EcNN201 that contains both the terminal alkene biosynthesis pathway and a two-component redox system well-characterized for *E. coli*. This redox system consists of an

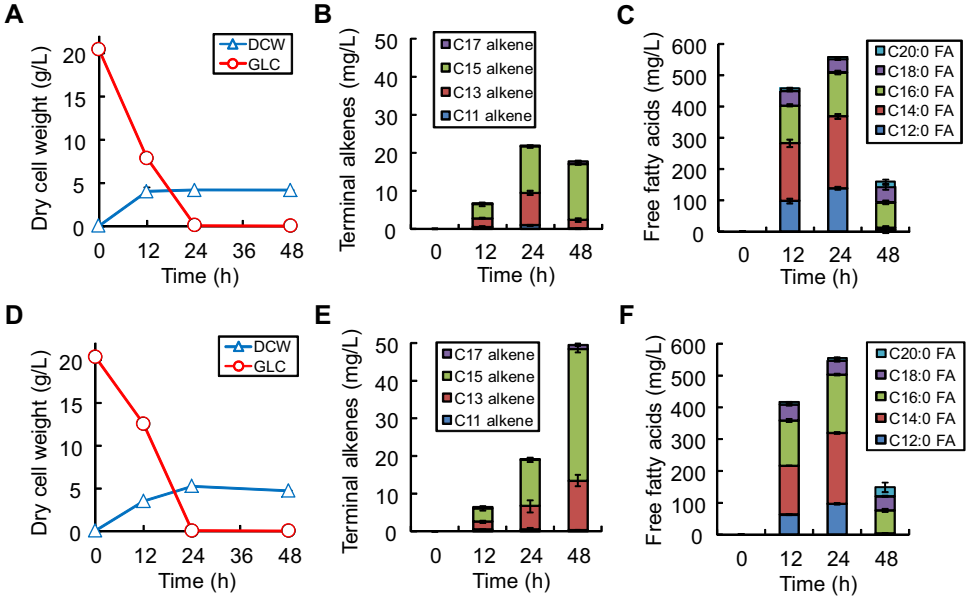

Fig. 3. Profiles of alkenes production in *E. coli* (**A-C**) EcNN101 and (**E-F**) and EcNN201. (**A, D**) Cell growth and glucose consumption, (**B, E**) Terminal alkene production, and (**C, F**) FA production.

NAD(P)H-dependent putidaredoxin reductase (CamA) and a [2Fe–2 S] putidaredoxin (CamB) transferring two electrons, one at a time, from NAD(P)H to the P450 enzyme (Peterson et al., 1990; Gunsalus and Sligar, 1978; Green et al., 2003).

Like EcNN101, EcNN201 could produce terminal alkenes during the growth phase (Fig. 3E). At 24 h, EcNN201 reached a cell concentration of 5.29 ± 0.05 g/L and entered the stationary phase after completely consuming 20 g/L glucose (Fig. 3D). EcNN201 exhibited slower growth and glucose consumption rates than EcNN101 during the growth phase likely due to metabolic burden from additional expression of a two component redox system. EcNN201 produced 19.25 ± 2.03 mg/L terminal alkenes, comparable to EcNN101. The composition of terminal alkenes produced by EcNN201 comprised of 2.4% ± 1.5% C11 alkene, 32.1% ± 5.8% C13 alkene, 64.3% ± 6.7% C15 alkene, and 1.2% ± 0.3% C17 alkene. Like EcNN101, EcNN201 produced a high amount of saturated FAs (556.12 ± 4.44 mg/L) consisting of 17.3% ± 0.3% C12:0 FA, 40.0% ± 0.5% C14:0 FA, 33.3% ± 0.3% C16:0 FA, 7.8% ± 0.4% C18:0 FA, and 1.6% ± 0.3% C20:0 FA (Fig. 3F). Overall, the terminal alkene production phenotypes were similar between EcNN101 and EcNN201 during the growth phase. This result implies that reducing equivalents were primarily channeled for ATP generation and biomass synthesis that are thermodynamically favorable under aerobic conditions, and hence likely became limited for decarboxylation to produce target alkenes.

However, during the stationary phase where glucose was not available, EcNN201 consumed a total amount of 407.45 ± 22.19 mg/L FAs for not only cell maintenance but also terminal alkene production. The terminal alkene production was increased up to 58% higher during the stationary phase than the growth phase, underlying the critical functional role of the redox system responsible for enhanced terminal alkene production. EcNN201 produced up to 49.64 ± 1.33 mg/L terminal alkenes, consisting of 0.7% ± 0.1% C11 alkene, 26.4% ± 2.6% C13 alkene, 70.7% ± 3.0% C15 alkene, and 2.2% ± 0.4% C17 alkene. At 48 h, the alkene titer and yield were 49.64 ± 1.33 mg/L and 2.44 ± 0.06 mg/g, respectively. In comparison to EcNN101, the terminal alkene production of EcNN201 increased by 2.8 fold. Based on the FA distributions at 24 and 48 h (Fig. 3F), we could infer that C12:0-C14:0 FAs were primarily degraded for cell maintenance and C16:0 FA utilized for alkene biosynthesis. This degradation phenotype is consistent with the distribution of terminal alkenes as well as the substrate preference of the endogenous FA synthetase FadD of *E. coli* responsible for catalyzing the first step of the β-oxidation (Kameda and Nunn, 1981).

The FA decarboxylation was clearly the rate-limiting step in our engineered terminal alkene biosynthesis pathway due to high accumulation of saturated FAs observed during the growth phase. The main cause of limited decarboxylation is inefficient electron transfer. We can observe that EcNN101 could not produce terminal alkenes during this stationary phase due to lack of the electron transfer to $OleT_{MC}$. This limitation could be overcome by introducing the two-component redox system in EcNN201. Specifically, the FA degradation during the stationary phase in EcNN201 generated high levels of reducing equivalents (i.e. NAD(P)H) via β-oxidation, and the redox system helped channel electrons to $OleT_{MC}$, thereby improving terminal alkene production.

EcNN201 produced terminal alkenes at a very comparable level to the recombinant *E. coli* harnessing the $OleT_{JE}$ decarboxylase from *Jeotgalicoccus* sp. (Liu et al., 2014). In our study, we did not observe EcNN101 and EcNN201 producing alkadienes even though unsaturated FAs were produced (Supplementary Fig. S4). Because the current terminal alkene production in EcNN201 is very inefficient, improving carbon and electron fluxes via metabolic engineering is critical for enhanced terminal alkene production in future study. In addition, controlling environmental conditions (e.g., sufficient supply of oxygen and use of highly reduced substrates) can potentially help improve terminal alkene production.

2.5. Using in silico protein modeling to illuminate the substrate specificity of $OleT_{MC}$ observed

Currently, it is not well understood why different FA decarboxylases have different substrate specificities. For instance, $OleT_{JE}$ prefers C12:0-C14:0 FAs to longer ones (Liu et al., 2014; Matthews et al., 2017) while $OleT_{MC}$ favors C16:0-C18:0 FAs more than shorter ones (this study). To better understand the underlying mechanism for governing the observed substrate preference of $OleT_{MC}$, we focused on analyzing its protein structure, using protein homology modeling, *in silico* residue mutation analysis, and docking simulation in combination with direct experimental evidence.

2.5.1. Construction of a 3-dimentional structure of $OleT_{MC}$.

We built a 3-dimensional (3D) structure of $OleT_{MC}$ using the version 2015.10 Molecular Operating Environment (MOE) software (MOE), based on the best-hit crystallographic structure of the substrate-bound (C20:0, arachidic acid) form of $OleT_{JE}$ (PDB:4L40 (Belcher et al., 2014), ~60% amino acid identity) as a template. The Ramachandran plot of $OleT_{MC}$ showed less than 0.5% of the residues to be in disallowed regions (Supplementary Fig. S5). Next, we superposed the heme-bound 3D structures of $OleT_{MC}$ and $OleT_{JE}$. Our result shows that these structures look almost identical (Fig. 5A) with the same catalytic site configuration (Fig. 5B).

2.5.2. Effect of binding free energy of $OleT_{MC}$ on its substrate preferences

To examine whether the binding free energy of FA-bound $OleT_{MC}$ might affect its substrate specificity, we docked $OleT_{MC}$ with various FAs (C10:0-C18:0) in MOE. Our result shows that the FA-bound $OleT_{MC}$ complexes exhibited the interactions between FAs and $OleT_{MC}$ where the binding pocket of $OleT_{MC}$ contains hydrophobic residues such as alanine (Ala, A), valine (Val, V), leucine (Leu, L), isoleucine (Ile, I), proline (Pro, P), phenylalanine (Phe, F) (Supplementary Figs. S6 and S7). The binding free energies of different FA-bound $OleT_{MC}$ complexes increase with shorter chain FAs (Fig. 4B). Remarkably, there is a strong linear correlation (R^2 = 0.92) between the binding free energies and specific activities of $OleT_{MC}$ for various FAs (Fig. 4C).

2.5.3. Residues at the tail of FA binding site are critical for determining the substrate specificity of $OleT_{MC}$

To identify the critical residues of the binding pocket that might affect the substrate specificity of $OleT_{MC}$, we first performed the alanine scan using the “alanine scan” tool in MOE. We scanned a set of 21 residues located at the FA docking sites of FA-bound $OleT_{MC}$ complexes (Supplementary Fig. S6A) by substituting each candidate with Ala residue. Regardless of C10:0-C18:0 FAs, we found that the mutation at P72A or I171A increased the stability, while F174A or F296A decreased the stability (Fig. 4D). In contrast, the mutation at I177A or V294A showed different stabilities for different FAs. Based on this first round of alanine scan and stability analysis, we narrowed the initial large set of 21 candidate residues to the 6 promising candidates, including P72, I171, F174, I177, F296 or V294, that might have a significant role for the substrate specificity of $OleT_{MC}$.

Next, we performed a comprehensive residue scan for these 6 candidate residues using the “residue scan” tool in MOE. Specifically, we generated a set of 54 $OleT_{MC}$ variants by systematically substituting each candidate with nine different hydrophobic residues including glycine (Gly, G), Ala, Val, Leu, Ile, Pro, Phe, methionine (Met, M), and tryptophan (Trp, W) and performed the stability analysis (Supplementary Figs. S8A-F). By determining the largest Δstability differences between C18:0 FA-bound and C10:0 FA-bound $OleT_{MC}$ complexes for each $OleT_{MC}$ variant, we could select a list of the top five mutants, including I177W, P72M, F296W, I177F, and P72F (Supplementary Fig. S8G), for detailed structure analysis.

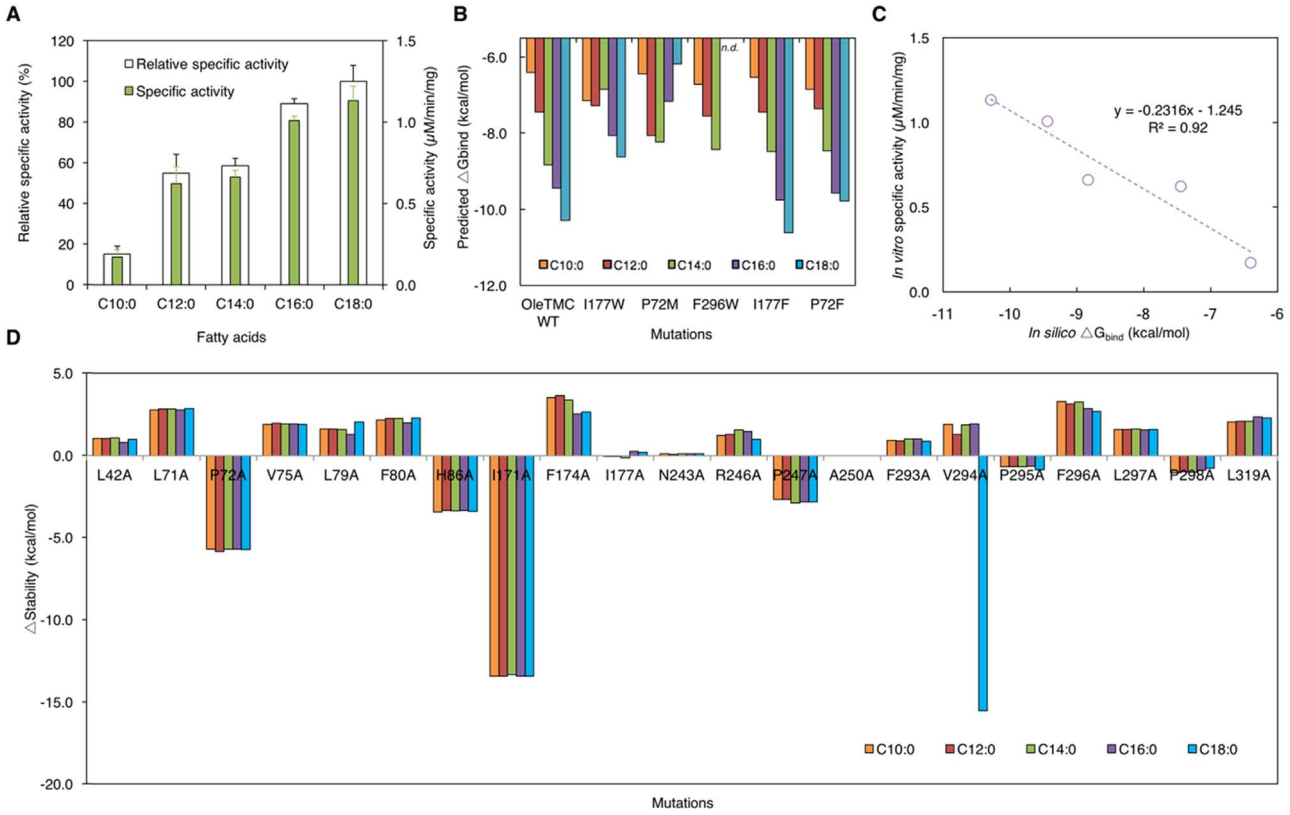

Fig. 4. (A) Specific and relative specific activities of $OleT_{MC}$ towards linear, saturated C10:0-C18:0 FAs. Each value is an average ± 1 standard deviation (n ≥ 2). **(B)** Comparison of predicted binding free energies for C10:0-C18:0 FAs between the $OleT_{MC}$ wildtype and mutants. **(C)** Correlation between in vitro specific activities and *in silico* binding free energies of $OleT_{MC}$ with various C10:0-C18:0 FAs. **(D)** *In silico* alanine scan of the potential FAs binding pocket with C10:0-C18:0 FAs-$OleT_{MC}$ complexes.

Interestingly, all these five $OleT_{MC}$ variants, selected by combination of alanine and residue scans, had the mutated residues located at the tail of the FA binding pocket (Figs. 5C-5H).

To determine whether the top 5 $OleT_{MC}$ variants are responsible for substrate preferences of $OleT_{MC}$, we next generated their 3D structures in MOE, followed by docking simulation of these variants with various FAs (C10:0-C18:0). Our result shows that the two variants, $OleT_{MC}$ P72M and F296W, significantly shifted substrate preferences while the other variants, $OleT_{MC}$ I177W, I177F, and P72F, did not (Fig. 5B). For the $OleT_{MC}$ F296W model, we observed that the correct docking poses, whose Arg246 should interact with the carboxylic functional group of FAs via hydrogen bonding, were no longer detected with C16:0 and C18:0 FAs. It has the lowest ΔG_{bind} of − 8.43 kcal/mol with C14:0 FA and the highest ΔG_{bind} of − 6.72 kcal/mol with C10:0 FA. Likewise, $OleT_{MC}$ P72M showed the lowest ΔG_{bind} of − 8.23 kcal/mol with C14:0 FA and the highest ΔG_{bind} of − 6.18 kcal/mol with C18:0 FA. These results suggest that P72M and F296W variants can shift the substrate preferences from longer to shorter FAs.

2.5.4. Reconfiguration of the binding pocket is responsible for shifting the substrate preference in $OleT_{MC}$ variants

To elucidate the underlying mechanism for shifting the substrate preference of $OleT_{MC}$, we compared the structures of $OleT_{MC}$ variants, including I177W (Fig. 5D), P72M (Fig. 5E), F296W (Fig. 5F), I177F (Fig. 5G), and P72F (Fig. 5H), and its wildtype (Fig. 5C). Our result shows that the disruption of the FA binding pockets affected substrate preferences of $OleT_{MC}$ P72M (Fig. 5E) and F296W (Fig. 5F). Specifically, they interfered with the access and docking of the longer C16:0-C18:0 FAs. Furthermore, since $OleT_{MC}$ F296W could not dock C16:0 and C18:0 FAs but $OleT_{MC}$ F72M could, it implies that the size of mutated residue (e.g. Trp (W) having a larger size than Met (M)) can play a significant role in changing the substrate specificity of $OleT_{MC}$.

Taken altogether, the residues at the tail of FA binding pocket of $OleT_{MC}$, such as P72 and F296, are critical for determining the substrate specificity of $OleT_{MC}$. Mutating these residues, instead of those at the catalytic site, can provide a promising protein engineering strategy to shift substrate specificity of $OleT_{MC}$ in future studies.

3. Conclusion

In this study, we demonstrated the direct biosynthesis of medium- and long-chain terminal alkenes in engineered *E. coli* strains from fermentable sugars. We found that the inefficient electron transfer in $OleT_{MC}$ was the rate limiting step that could be overcome by introducing a two-component redox system. Together with the homology protein modeling, *in silico* residue mutation analysis, and docking simulation with direct experimental evidence, we proposed the underlying mechanism that determines the substrate preferences of $OleT_{MC}$. Overall, this study provides a better understanding of the novel functions of FA decarboxylases and helps lay out a foundation for future protein and metabolic engineering to modulate fatty acid thioesterases and $OleT_{MC}$ specificities to produce designer terminal alkenes with desirable carbon chain characteristics.

4. Materials and methods

4.1. Bacterial strains and plasmids

Table 1 shows a list of bacterial strains and plasmids used in this study. *E. coli* TOP10 was used for molecular cloning while BL21 (λDE3) was employed as an expression and characterization host. All plasmids were constructed by using a modified pETite* (Layton and Trinh, 2014), a derivative of pETite C-His backbone vector (Lucigen Corp., WI, USA), suitable for the BglBricks gene assembly method

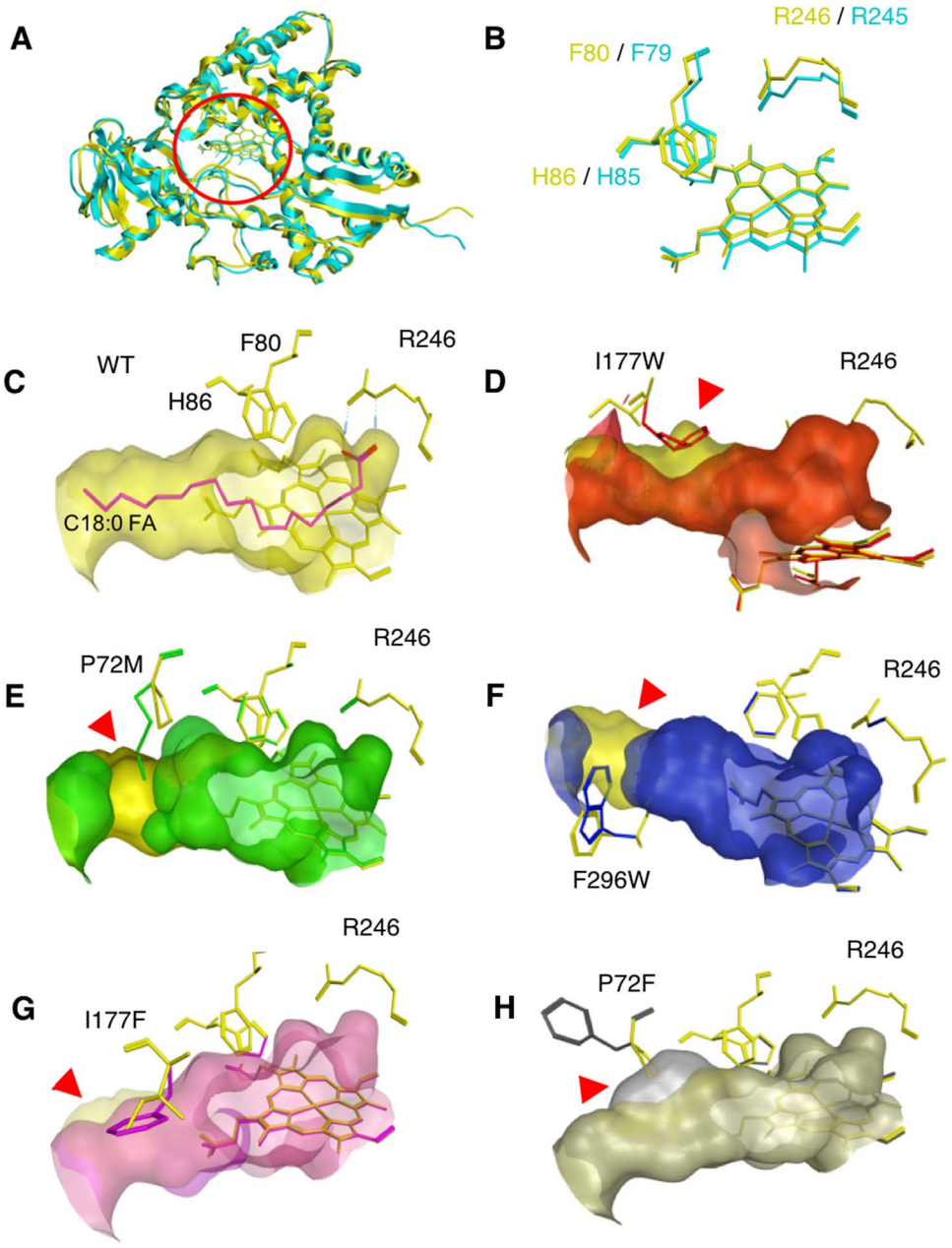

Fig. 5. (A) Comparison of the protein structures between the homology model of $OleT_{MC}$ (in yellow) and the crystal structure of C20:0 FA-bound $OleT_{JE}$ (in cyan; PDB:4L40). **(B)** Overlay of the catalytic site structures of $OleT_{MC}$ (in yellow) and $OleT_{JE}$ (in cyan). **(C)** A homology model of $OleT_{MC}$ docked with C18:0 FA. **(D-H)** Overlay of the potential FA binding pocket of the wildtype $OleT_{MC}$ (in yellow) and the $OleT_{MC}$ variants including **(D)** I177W (in red), **(E)** P72M (in blue), **(F)** F296W (in purple), **(G)** I177F (in pink), and **(H)** P72F (in gray). Red circle indicates the location of the FA binding pocket in OleT. Filled red triangles point to the distinctive features in the FA binding pockets of the $OleT_{MC}$ variants as compared to the wildtype.

(Anderson et al., 2010). Primers used to construct the plasmids in this study are listed in Table 2.

To construct the plasmid pCT71, the leaderless *tesA** was amplified from the genomic DNA of *E. coli* MG1655 using the primers mw.24 f/p064_r, and inserted into pETite* via the *Nde*I/*Xho*I sites. The gene *tesA** was derived from *tesA* whose leader peptide sequence was removed to keep the encoded protein TesA* localized in the cytosol (Cho and Cronan, 1995). The plasmid pNN33 was constructed by the Gibson gene assembly method (Gibson, 2009) using 2 DNA fragments: i) the decarboxylase gene $OleT_{MC}$ amplified from the genomic DNA of *M. caseolyticus* using the primers Nhis6_$OleT_{MC}$F/Nhis6_$OleT_{MC}$R and ii) the backbone fragment amplified from pETite* using the primers pnn33_Nhis6F/pnn33_Nhis6R. To construct the plasmid pNN32, $OleT_{MC}$ was amplified using the primers mc_decarbF/rev_decarb and inserted into pCT71 via the *Bam*HI/*Xho*I sites. The plasmid pNN34 was constructed by the Gibson gene assembly method using 3 DNA fragments: i) *camA* gene amplified from the genomic DNA of *P. putida* using the primers pnn82/pnn83, ii) *camB* amplified from the genomic DNA of *P. putida* using the primers pnn84/pnn85, and iii) the backbone fragment amplified from pETite* using the primers pETiteF/pETiteR. All plasmid constructs were confirmed by enzyme digestion, PCR amplification of the respective genes, and sequencing.

The strain EcNN101 was generated by introducing pNN32 into BL21 (λDE3) via electroporation. Similarly, the strain EcNN201 was created by co-transforming pNN32 and pNN34 into BL21 (λDE3).

4.2. Medium and strain characterization

4.2.1. Medium

For molecular cloning and protein expression, Luria-Bertani (LB)

Table 1
List of strains and plasmids.

Strains/ plasmids	Genotype	Sources
Strains		
P. putida	Wildtype	ATCC17453
M. caseolyticus	Wildtype	ATCC13548
TOP10	*F⁻ mcrA Δ(mrr-hsdRMS-mcrBC) φ80lacZΔM15 ΔlacX74 nupG recA1 araD139 Δ(ara-leu)7697 galE15 galK16 rpsL(Str^R) endA1 λ⁻*	Invitrogen
BL21 (λDE3)	*F⁻ ompT hsdS$_B$ (r$_B$⁻ m$_B$⁻) gal dcm (λDE3)*	Invitrogen
EcNN101	BL21 (λDE3) carrying pNN32	This study
EcNN201	BL21 (λDE3) carrying pNN32 and pNN34	This study
Plasmids		
pETite C-His	pBR322 *ori*; kan^R	Lucigen
pETite*	kan^R	Layton 2014
pCT71	pETite* P$_{T7}$::*tesA**::T$_{T7}$; kan^R	This study
pNN33	pETite* P$_{T7}$::*oleT$_{MC}$*::T$_{T7}$; kan^R	This study
pNN32	pETite* P$_{T7}$::*tesA**::*oleT$_{MC}$*::T$_{T7}$; kan^R	This study
pNN34	pETite* P$_{T7}$::*camAB*::T$_{T7}$; amp^R	This study

Table 2
List of primers.

Primers	Primer sequence (5′ to 3′)
mw.24 f	AAA AAA CAT ATG GCG GAC ACG TTA TTG ATT CT
p064_r	AAA AAA CTC GAG TTA GGA TCC TTA TGA GTC ATG ATT TAC TAA AG
Nhis6_OleT$_{MC}$F	AGA AGG AGA TAT ACA TAT GCA TCA TCA CCA CCA TCA CAG TAA AAG AGT TCC TAA AGA TAG
Nhis6_OleT$_{MC}$R	GTT ATG CTA GTT ATT GCT CAG CGG TGG CGG CCG CTC TAT TAT TTT GTA CGG TCG ATA TTC
pnn33_Nhis6F	TAA TAG AGC GGC CGC CAC
pnn33_Nhis6R	GTG ATG GTG GTG ATG ATG CAT ATG TAT ATC TCC TTC TTA TAG TTA AAC AAA ATT AT
mc_DecarbF	ATG GAT CCA AAA ATG AGG GTA GAG TTT ACT ATT AA
rev-Decarb	ATC TCG AGT TAT TTT GTA CGG TCG ATA TTC ACC CT
pnn82	ATA ATT TTG TTT AAC TAT AAG AAG GAG ATA TAC ATA TGA ACG CAA ACG ACA ACG TGG TC
pnn83	GAC ACA TAC ACT ACT TTA GAC ATT TAT ATC TCC TTT CAG GCA CTA CTC AGT TCA GCT TT
pnn84	AAA GCT GAA CTG AGT AGT GCC TGA AAG GAG ATA TAA ATG TCT AAA GTA GTG TAT GTG TC
pnn85	GTG ATG ATG CTC GAG TTA GGA TCC TTA CCA TTG CCT ATC GGG AAC ATC
pETiteF	GGA TCC TAA CTC GAG CAT CAT CAC CAC CAT CAC TA
pETiteR	TAT ATC TCC TTC TTA TAG TTA AAC AAA ATT ATT TC

medium containing 5 g/L yeast extract, 10 g/L tryptone, 5 g/L NaCl, and antibiotics (if applicable) was used for *E. coli* and *P. putida* cultures. The medium for cultivating *M. caseolyticus* was comprised of 5 g/L glucose, 5 g/L yeast extract, 10 g/L casein peptone, and 5 g/L NaCl. The hybrid M9 medium used for strain characterization contained 1X M9 salt solution (Sambrook, 2001), 1 mM $MgSO_4$, 10 mM $CaCl_2$, 1 mL/L stock trace metals solution, 5 g/L yeast extract, 20 g/L glucose, and appropriate antibiotics (e.g., 50 μg/mL kanamycin or 100 μg/mL ampicillin for single plasmid selection or 25 μg/mL kanamycin plus 50 μg/mL ampicillin for double plasmid selection) (Trinh et al., 2011).

4.2.2. Strain characterization

For terminal alkene production experiments, single colonies were inoculated in 15 mL tubes containing 8 mL of LB medium and incubated in a rotary shaker at 37 °C with a shaking rate of 175 rpm for 12 h (h). The overnight seed culture was then transferred into the hybrid M9 medium with an initial $OD_{600\,nm}$ ~0.05 in 500 mL baffled shake flasks with a 100 mL working volume. When reaching the exponential phase of $OD_{600\,nm}$ ~0.6, the cell culture was first supplemented with 1 mM 5-aminolevulinic acid (ALA) to enhance the yield of active P450 (Jansson et al., 2000), followed by IPTG induction at a working concentration of 0.5 mM, and run for a total of 48 h. Samples were collected for determining cell growth, substrate consumption, and product formation. All experiments were performed in biological triplicates.

4.3. Enzyme expression, purification, and characterization

BL21 (λDE3) pNN33 was used to express $OleT_{MC}$ His-tagged at the N-terminus in LB medium at 20 celcius (°C). Exponentially grown cells ($OD_{600\,nm}$ ~0.6) were induced with IPTG at a working concentration of 0.5 mM. After 20 h, cells were collected, washed, and resuspended in 50 mM phosphate buffer (pH 7.5). The resuspended cells were disrupted by ultrasonication with a sonic dismembrator (Model # FB120, Thermo Fisher Scientific Inc., MA, USA) and then centrifuged at 13,500 rcf for 20 min at 4 °C to collect the soluble crude cell extract for downstream protein purification. The sonication protocol was set with 70% amplitude with cycles of 5 s ON/10 s OFF pulses on ice for 15 min.

The expressed $OleT_{MC}$ protein was semi-purified by the HisPur Ni-NTA Spin column (cat # PI88224, Thermo Fisher Scientific, MA, USA) according to the manufacturer's instruction. Following incubation for 1 h at 4 °C, the resin was washed three times with wash buffer (20 mM of imidazole) and the His-tagged $OleT_{MC}$ was eluted from the resin by adding elution buffer (500 mM of imidazole). Then, the final protein sample was concentrated using Amicon Ultra centrifugal filters (cat # UFC801024, Merck, NJ, USA). The purified protein was analyzed by the 12% SDS-PAGE and the protein concentration was determined by the Bradford assay (Bradford, 1976).

To quickly test the active form of $OleT_{MC}$ (i.e., the actual heme content of P450 protein), the spectrophotometric carbon monoxide (CO) difference spectral analysis was routinely carried out to determine the maximum characteristic absorbance at 450 nm (Omura and Sato, 1964). First, 0.5 mL of 20 mg/mL purified protein sample was diluted in 4.5 mL of 50 mM Tris-HCl buffer (pH 7.6) containing 1 mM EDTA and 10% (v/v) glycerol. The solution was then supplemented with a few crystals of sodium dithionite and saturated with ~30–40 bubbles of CO at a rate of 1 bubble per second. The maximum spectrophotometric absorbance peak at 450 nm indicates the reduced P450 complexed with CO and hence confirms the enzymatic catalytic center of $OleT_{MC}$ is active.

The H_2O_2-independent FA decarboxylase activity of $OleT_{MC}$ was characterized in vitro with various linear, saturated C8:0-C20:0 FAs. Each reaction assay has a working volume of 500 μL that contained 1 mM NADH, 10 μM spinach ferredoxin (cat. # F3013, Sigma Aldrich, CA, USA), 0.5 unit spinach ferredoxin reductase (cat. # F0628, Sigma Aldrich, CA, USA), 20 μg/mL purified $OleT_{MC}$, and 0.05 mM FAs. The assay was conducted at 37 °C for 60 min. After the reaction, alkenes were extracted with ethyl acetate, and analyzed by gas chromatography coupled with mass spectrometry.

4.4. Analytical methods

4.4.1. Cell growth

Cell optical density was measured at $OD_{600\,nm}$ using a spectrophotometer (Spectronic 20 +, Thermo Fisher Scientific, MA, USA). The correlation between the cell optical density and dry cell weight (DCW) was determined to be 1 $OD_{600\,nm}$ = 0.48 g DCW/L.

4.4.2. High performance liquid chromatography (HPLC)

The HPLC Shimadzu system equipped with a BioRad Aminex HPX 87-H column (cat # 1250140, BioRad, CA, USA) and both RID and UV–VIS detectors (Shimadzu Scientific Instruments, Inc., MD, USA) were used to quantify extracellular metabolites (e.g., glucose, organic acids, and alcohols). The running method used 10 mN H_2SO_4 as a mobile phase operated at a flow rate of 0.6 mL/min and an oven temperature set at 48 °C (Trinh et al., 2008).

4.4.3. Gas chromatography coupled with mass spectroscopy (GC/MS)

For FAs analysis, sample preparation and GC/MS methods were described previously (Wierzbicki et al., 2016). For terminal alkene analysis, 500 µL of samples (cells plus supernatants) were transferred to a 2 mL polypropylene microcentrifuge tube with a screw cap containing 100–200 mg of glass beads (0.25–0.30 mm in diameter), 60 µL of 6 N HCl, and 500 µL of ethyl acetate solution containing 1 mg/L of ethyl pentadecanoate as an internal standard. The cells were lysed by bead bashing for 4 min using a Biospec Mini BeadBeater 16 and then centrifuged at 13,300 g for 2 min. The extractants of the organic layer were used for the GC/MS analysis. All alkenes were analyzed by using HP6890 GC/MS system equipped with a 30 m x 0.25 mm i.d. 0.25 µm film thickness column plus an attached 10 m guard column (Zebron ZB-5, Phenomenex Inc.) and a HP 5973 mass selective detector. An electron ionization in scan mode (50–650 *m/z*) method was deployed to analyze 1 µL of samples. The column temperature was initially held at 50 °C for 1 min, increased by 20 °C/min until 300 °C, and held for 2 min. Helium was used as a carrier gas and run at 1 mL/min. The mass transfer line and ion source were set at 250 °C and 200 °C, respectively.

4.5. Bioinformatics

For sequence alignment and phylogenetic analysis, protein sequences were retrieved from the National Center for Biotechnology Information (NCBI), and were inputted into MEGA7 (Kumar et al., 2016) and aligned via MUSCLE (Edgar, 2004). The phylogenetic tree was generated using the neighbor-joining algorithm with a 1000 bootstrap value. BLASTp was used to calculate the identity of sequences (Altschul et al., 1990) using $OleT_{JE}$ as the template.

4.6. Construction of a 3-dimentional structure and in silico analysis of $OleT_{MC}$

4.6.1. Homology modeling

The 3D structure of $OleT_{MC}$ was generated by the homology modeling function in MOE (Molecular Operating Environment software, version 2015.10) (MOE). To obtain the heme-bound protein structure, the reference substrate, heme, was first extracted from the best hit, substrate-bound crystallographic structure of $OleT_{JE}$ (PDB:4L40) and then added to the homology model of $OleT_{MC}$. Next, the heme-bound model of $OleT_{MC}$ generated was optimized by energy minimization using the Amber10: EHT (Extended Huckel Theory) force field (Corbeil et al., 2012; Case et al., 2005). The Ramachandran plot analysis was performed to determine the overall stereochemical property of the protein model.

4.6.2. Docking simulation

To dock various FAs with the heme-bound homology model of $OleT_{MC}$, the 3D structures of various C10:0-C18:0 FAs were first generated by modifying C20:0 FA extracted from $OleT_{JE}$ (PDB:4L40) with the '3D builder' tool of MOE and then optimized by energy minimization using the Amber10: EHT force field. Next, the "site finder" tool of MOE was used to search for potential binding sites. Upon identifying the site consistent with the reported catalytic site of $OleT_{JE}$ (Matthews et al., 2017), dummy atoms were generated to mark potential binding sites. To select the exclusive potential binding site of FA, we also removed some dummy atoms located near heme. Finally, we added the target C10:0-C18:0 FAs to the binding site of the heme-bound homology model of $OleT_{MC}$. All structures were protonated using the "protonate3D" tool of MOE prior to docking simulation.

Docking simulations were carried out as previously described (Liu et al., 2016). In brief, the induced fit docking protocol employed the Triangle Matcher placement method and the London ΔG scoring function. In our docking simulations, we performed 30 docking interactions for each FA substrate. The binding free energy (ΔG_{bind}, in kcal/mol) for each binding pose was then minimized using the Amber10: EHT force field and rescored with the GBVI/WSA ΔG scoring function (Corbeil et al., 2012). The best scored pose, exhibiting the crucial interaction between the residue Arg246 and carboxylic functional group of the substrate via hydrogen bonding (Matthews et al., 2017) at root-mean-square-deviation (RMSD) < 2 Å, was selected for further analysis. The "surface and maps" tool of MOE was employed to visualize the molecular surface of atoms in the potential FA binding site.

4.6.3. In silico mutation analysis

The "alanine scan" and the "residue scan" tools in MOE were used for *in silico* mutation analysis of FA-$OleT_{MC}$ complexes. Specifically, the alanine scanning technique (Massova and Kollman, 1999; Morrison and Weiss, 2001) was employed to determine the importance of a specific residue to the stability, affinity, and/or property of the FA-$OleT_{MC}$ complexes upon being substituted with Ala in the binding pocket. Residue scanning technique, also known as site-directed mutagenesis (Eriksen et al., 2014), was applied to generate large number of $OleT_{MC}$ variants for the comprehensive mutation study using the selected residues from the alanine scan. By utilizing these tools, we could replace each of the interface residues with a specific residue of interest and calculates the effect of the mutation on the binding free energy (ΔG_{bind}) of the complexes. The ΔStability values (kcal/mol) were calculated as the relative binding free energy difference ($\Delta\Delta G_{bind}$) between the mutant (ΔG_{mutant}) and wildtype ($\Delta G_{wildtype}$) in MOE.

Acknowledgements

We would like to thank Dr. Fu-min Menn (Center of Environmental Biotechnology, UTK) for his assistance in developing the GC/MS method, Dr. Jerome Baudry (UTK) for accessing the MOE software, Dr. Donovan Layton (UTK) for assistance with GC/MS and bioinformatics analyses, and members of Trinh lab for proofreading and providing critical comments on the manuscript.

Funding

This research was supported by the laboratory start-up, SEERC, and JDRD seed funds from the University of Tennessee, Knoxville (UTK), a NSF CAREER award (NSF#1553250 to CTT), and a DOE subcontract grant from the Center of Bioenergy Innovation (CBI), the U.S. Department of Energy Bioenergy Research Center funded by the Office of Biological and Environmental Research in the DOE Office of Science (DE-AC05-00OR22725).Conflict of interest statement

None declared.

Appendix A. Supporting information

Supplementary data associated with this article can be found in the online version at doi:10.1016/j.mec.2018.e00076.

References

Altschul, S.F., Gish, W., Miller, W., Myers, E.W., Lipman, D.J., 1990. Basic local alignment search tool. J. Mol. Biol. 215, 403–410.

Anderson, J.C., Dueber, J., Leguia, M., Wu, G., Goler, J., Arkin, A., Keasling, J., 2010. BglBricks: a flexible standard for biological part assembly. J. Biol. Eng. 4, 1.

Belcher, J., McLean, K.J., Matthews, S., Woodward, L.S., Fisher, K., Rigby, S.E., Nelson, D.R., Potts, D., Baynham, M.T., Parker, D.A., 2014. Structure and biochemical properties of the alkene producing cytochrome P450 OleTJE (CYP152L1) from the Jeotgalicoccus sp. 8456 bacterium. J. Biol. Chem. 289, 6535–6550.

Beller, H.R., Goh, E.-B., Keasling, J.D., 2010. Genes involved in long-chain alkene biosynthesis in Micrococcus luteus. Appl. Environ. Microbiol. 76, 1212–1223.

Bonner, W.M., Bloch, K., 1972. Purification and properties of fatty acyl thioesterase I from Escherichia coli. J. Biol. Chem. 247, 3123–3133.

Bradford, M., 1976. A rapid and sensitive method for the quantitation of microgram quantitites of protein utilizing the principle of protein-dye binding. Anal. Biochem. 72, 248–254.
Case, D.A., Cheatham, T.E., 3rd, Darden, T., Gohlke, H., Luo, R., Merz, K.M., Jr., Onufriev, A., Simmerling, C., Wang, B., Woods, R.J., 2005. The Amber biomolecular simulation programs. J. Comput. Chem. 26, 1668–1688.
Chen, B., Lee, D.-Y., Chang, M.W., 2015. Combinatorial metabolic engineering of Saccharomyces cerevisiae for terminal alkene production. Metab. Eng. 31, 53–61.
Cho, H., Cronan, J.E., 1995. Defective export of a periplasmic enzyme disrupts regulation of fatty acid synthesis. J. Biol. Chem. 270, 4216–4219.
Corbeil, C.R., Williams, C.I., Labute, P., 2012. Variability in docking success rates due to dataset preparation. J. Comput. Aided Mol. Des. 26, 775–786.
Dennig, A., Kuhn, M., Tassoti, S., Thiessenhusen, A., Gilch, S., Bülter, T., Haas, T., Hall, M., Faber, K., 2015. Oxidative decarboxylation of short-chain fatty acids to 1-alkenes. Angew. Chem. Int. Ed. 54, 8819–8822.
Edgar, R.C., 2004. MUSCLE: multiple sequence alignment with high accuracy and high throughput. Nucleic Acids Res. 32, 1792–1797.
Eriksen, D.T., Lian, J.Z., Zhao, H.M., 2014. Protein design for pathway engineering. J. Struct. Biol. 185, 234–242.
Gibson, D.G., 2009. Synthesis of DNA fragments in yeast by one-step assembly of overlapping oligonucleotides. Nucleic Acids Res. 37, 6984–6990.
Görgen, G., Frößl, C., Boland, W., Dettner, K., 1990. Biosynthesis of 1-alkenes in the defensive secretions ofTribolium confusum (Tenebrionidae); stereochemical implications. Experientia 46, 700–704.
Green, A.J., Munro, A.W., Cheesman, M.R., Reid, G.A., von Wachenfeldt, C., Chapman, S.K., 2003. Expression, purification and characterisation of a Bacillus subtilis ferredoxin: a potential electron transfer donor to cytochrome P450 BioI. J. Inorg. Biochem. 93, 92–99.
Gunsalus, I., Sligar, S., 1978. Oxygen reduction by the P450 monoxygenase systems. Adv. Enzymol. Relat. Areas Mol. Biol. 47, 1–44.
Jansson, I., Stoilov, I., Sarfarazi, M., Schenkman, J.B., 2000. Enhanced expression of CYP1B1 in Escherichia coli. Toxicology 144, 211–219.
Kameda, K., Nunn, W., 1981. Purification and characterization of acyl coenzyme A synthetase from Escherichia coli. J. Biol. Chem. 256, 5702–5707.
Kumar, S., Stecher, G., Tamura, K., 2016. MEGA7: molecular evolutionary genetics analysis version 7.0 for bigger datasets. Mol. Biol. Evol. 33, 1870–1874.
Ladygina, N., Dedyukhina, E., Vainshtein, M., 2006. A review on microbial synthesis of hydrocarbons. Process Biochem. 41, 1001–1014.
Lappin, G.R., Sauer, J.D., 1989. Alpha Olefins Applications Handbook 37. CRC Press.
Layton, D.S., Trinh, C.T., 2014. Engineering modular ester fermentative pathways in *Escherichia coli*. Metab. Eng. 26, 77–88.
Liu, M., Zheng, N., Li, D., Zheng, H., Zhang, L., Ge, H., Liu, W., 2016. cyp51A-based mechanism of azole resistance in Aspergillus fumigatus: Illustration by a new 3D Structural model of Aspergillus fumigatus CYP51A protein. Med. Mycol. 54, 400–408.
Liu, Y., Wang, C., Yan, J., Zhang, W., Guan, W., Lu, X., Li, S., 2014. Hydrogen peroxide-independent production of α-alkenes by OleTJE P450 fatty acid decarboxylase. Biotechnol. Biofuels 7, 28.
Massova, I., Kollman, P.A., 1999. Computational alanine scanning to probe protein-protein interactions: a novel approach to evaluate binding free energies. J. Am. Chem. Soc. 121, 8133–8143.
Matthews, S., Belcher, J.D., Tee, K.L., Girvan, H.M., McLean, K.J., Rigby, S.E., Levy, C.W., Leys, D., Parker, D.A., Blankley, R.T., Munro, A.W., 2017. Catalytic determinants of alkene production by the cytochrome P450 peroxygenase OleTJE. J. Biol. Chem. 292, 5128–5143.
Mendez-Perez, D., Begemann, M.B., Pfleger, B.F., 2011. Modular synthase-encoding gene involved in α-Olefin biosynthesis in Synechococcus sp. strain PCC 7002. Appl. Environ. Microbiol. 77, 4264–4267.
Mendez-Perez, D., Herman, N.A., Pfleger, B.F., 2014. A desaturase gene involved in the formation of 1, 14-nonadecadiene in Synechococcus sp. strain PCC 7002. Appl. Environ. Microbiol. 80, 6073–6079.
MOE. Molecular Operating Environment (MOE), Chemical Computing Group ULC, 1010 Sherbooke St. West, Suite #910, Montreal, QC, Canada, H3A 2R7.
Mol, J., 2004. Industrial applications of olefin metathesis. J. Mol. Catal. A: Chem. 213, 39–45.
Morrison, K.L., Weiss, G.A., 2001. Combinatorial alanine-scanning. Curr. Opin. Chem. Biol. 5, 302–307.
Ney, P., Boland, W., 1987. Biosynthesis of 1-alkenes in higher plants. Eur. J. Biochem. 162, 203–211.
Omura, T., Sato, R., 1964. The carbon monoxide-binding pigment of liver microsomes. I. Evidence for its hemoprotein nature. J. Biol. Chem. 239, 2370–2378.
Peterson, J., Lorence, M., Amarneh, B., 1990. Putidaredoxin reductase and putidaredoxin. cloning, sequence determination, and heterologous expression of the proteins. J. Biol. Chem. 265, 6066–6073.
Ren, T., Patel, M., Blok, K., 2006. Olefins from conventional and heavy feedstocks: energy use in steam cracking and alternative processes. Energy 31, 425–451.
Rude, M.A., Baron, T.S., Brubaker, S., Alibhai, M., Del Cardayre, S.B., Schirmer, A., 2011. Terminal olefin (1-alkene) biosynthesis by a novel p450 fatty acid decarboxylase from *Jeotgalicoccus* species. Appl. Environ. Microbiol. 77, 1718–1727.
Rui, Z., Li, X., Zhu, X., Liu, J., Domigan, B., Barr, I., Cate, J.H.D., Zhang, W., 2014. Microbial biosynthesis of medium-chain 1-alkenes by a nonheme iron oxidase. Proc. Natl. Acad. Sci. 111, 18237–18242.
Rui, Z., Harris, N.C., Zhu, X., Huang, W., Zhang, W., 2015. Discovery of a family of desaturase-Like enzymes for 1-Alkene biosynthesis. ACS Catal. 5, 7091–7094.
Sambrook, J., 2001. Molecular Cloning: a Laboratory Manual. Cold Spring Harbor Laboratory Press.
Tornabene, T., 1982. Microorganisms as hydrocarbon producersNew Trends in Research and Utilization of Solar Energy through Biological Systems. Springer, 49–52.
Trinh, C.T., Unrean, P., Srienc, F., 2008. Minimal Escherichia coli cell for the most efficient production of ethanol from hexoses and pentoses. Appl. Environ. Microbiol. 74, 3634–3643.
Trinh, C.T., Li, J., Blanch, H.W., Clark, D.S., 2011. Redesigning Escherichia coli metabolism for anaerobic production of isobutanol. Appl. Environ. Microbiol 77, 4894–4904.
Wierzbicki, M., Niraula, N., Yarrabothula, A., Layton, D.S., Trinh, C.T., 2016. Engineering an Escherichia coli platform to synthesize designer biodiesels. J. Biotechnol. 224, 27–34.
Winters, K., Parker, P., Van Baalen, C., 1969. Hydrocarbons of blue-green algae: geochemical signfficance. Science 163, 467–468.
Zhu, Z., Zhou, Y.J., Kang, M.-K., Krivoruchko, A., Buijs, N.A., Nielsen, J., 2017. Enabling the synthesis of medium chain alkanes and 1-alkenes in yeast. Metab. Eng. 44, 81–88.